IEEE Access
Multidisciplinary | Rapid Review | Open Access Journal

Received May 10, 2020, accepted June 3, 2020, date of publication June 11, 2020, date of current version June 24, 2020.

Digital Object Identifier 10.1109/ACCESS.2020.3001652

Evaluation of Efficacy of Fungicides for Control of Wheat Fusarium Head Blight Based on Digital Imaging

DONGYAN ZHANG[1], ZHICUN WANG[1], NING JIN[2,3], CHUNYAN GU[4], YU CHEN[4], AND YANBO HUANG[5]

[1]National Engineering Research Center for Agro-Ecological Big Data Analysis and Application, Anhui University, Hefei 230601, China
[2]Department of Resources and Environment, Shanxi Institute of Energy, Jinzhong 030600, China
[3]Key Laboratory of Geospatial Technology for Middle and Lower Yellow River Regions, Ministry of Education, Henan University, Kaifeng 475004, China
[4]Institute of Plant Protection and Agro-Products Safety, Anhui Academy of Agricultural Sciences, Hefei 230031, China
[5]USDA-ARS, Crop Production Systems Research Unit, Stoneville, MS 38776, USA

Corresponding authors: Yu Chen (chenyu@aaas.org.cn) and Yanbo Huang (yanbo.huang@usda.gov)

This work was supported in part by the National Natural Science Foundation of China under Grant 41771463 and Grant 41771469, in part by the Anhui Provincial Major Science and Technology Projects under Grant 18030701209, and in part by the National Key Research and Development Program of China under Grant 2016YFD0300700.

ABSTRACT Fusarium head blight (FHB) is one of the most important diseases in wheat worldwide. Evaluation and identification of effective fungicides are essential for control of FHB. However, traditional methods based on the manual disease severity assessment to evaluate the efficacy of fungicides are time-consuming and laborsome. In this study, we developed a new method to rapidly assess the severity of FHB and evaluate the efficacy of fungicide application programs. Enhanced red-green-green (RGG) images were processed from acquired raw red-green-blue (RGB) images of wheat ear samples; the images were transformed in color spaces through K-means clustering for rough segmentation of wheat ears; a random forest classifier was used with features of color, texture, geometry and vegetation index for fine segmentation of disease spots in wheat ears; a newly proposed width mutation counting algorithm was used to count wheat ears; and the disease severity of the wheat ears groups was graded and the efficacy of six fungicides was evaluated. The results show that the segmentation algorithm could segment wheat ears from a complex field background. And the counting algorithm could effectively solve the problem of wheat ear adhesion and occlusion. The average counting accuracy of all and diseased wheat ears were 93.00% and 92.64%, respectively, with the coefficients of determination (R^2) of 0.90 and 0.98, and the root mean square error (RMSE) of 10.56 and 7.52, respectively. The new method could accurately assess the diseased levels of wheat eat groups infected by FHB and determine the efficacy of the six fungicides evaluated. The results demonstrate a potential of using digital imaging technology to evaluate and identify effective fungicides for control of the FHB disease in wheat and other crop diseases.

INDEX TERMS Fusarium head blight, K-means clustering, random forest, width mutation counting algorithm, fungicide spraying.

I. INTRODUCTION

Wheat is one of the world's major food crops, providing essential nutrients for human life [1]. Its adequate supply is essential to ensure global food security [2], [3]. Fusarium head blight (FHB), caused by *Fusarium graminearum*, is a devasting disease in wheat that occurs worldwide [4], [5]. FHB can cause metamorphism of the whole wheat grains [6] and reduce yield and quality of wheat. The fungus also produces deoxynivalenol (DON), a toxin that can cause poisoning to humans and animals [7]. Therefore, it is very important to develop effective strategies to monitor the development of FHB and control of the disease. At present, control of FHB is still primarily through the use of chemical fungicides [8]. Therefore, evaluating the efficacy of fungicides is the first essential step in developing effective fungicide application programs that can control the FHB disease.

The associate editor coordinating the review of this manuscript and approving it for publication was Yakoub Bazi.

There are two important steps in assessing the FHB disease by using digital images: image segmentation for wheat ears and wheat ear counting [9]–[11]. Through literature research it was found that image processing alone and its integration with machine learning are commonly used to achieve the two steps [12]–[14]. For example, Fernandez-Gallego *et al.* used image filtering technique to complete wheat ear image segmentation and wheat ear counting [15]. Their counting accuracy was higher than 90%. Cointault *et al.* used image textural features to detect wheat ears, and the average counting error was 6% [16]. Liu *et al.* used the color and textural features of images to segment wheat ears. Then they counted wheat ears by extracting wheat ear skeleton, and the counting accuracy was 95.77% [17]. Fan *et al.* extracted the color and textural features of wheat ears and used support vector machine (SVM) classifiers to segment wheat ears. The average counting accuracy was 93.1% [18]. Zhao *et al.* used color features and Adaboost algorithm to detect wheat ears, and the counting accuracy was about 88.7% [19]. Liu *et al.* used the improved K-means algorithm to count wheat ears and the counting accuracy was 94.69% [20]. Zhou *et al.* used multi-sensor fusion and an improved maximum entropy segmentation algorithm to achieve great results of segmentation and counting of wheat ears [21]. The multi-sensor images, however, were difficult to obtain.

In recent years, deep learning method has been introduced into object segmentation and object counting [22], [23]. Compared to conventional algorithms of machine learning, although the accuracy of deep learning is normally high, it needs many more samples and much more time for model training [24]–[29]. In addition, data annotation is a time-consuming and laborious task during the process of preparing data set [25]. For example, Zhang *et al.* designed a wheat ears detection and counting system based on convolutional neural networks (CNNs) [26]. And the overall recognition rate was as high as 99.6% with 39,338 images [26]. Sadeghi-Tehran *et al.* used simple linear iterative clustering and deep CNNs to segment wheat ears from original images in a field background [27]. And the coefficient of determination (R^2) between prediction number and true number reached 0.94 with 24,938 wheat ears and 30,639 manually annotated backgrounds [27]. Michael *et al.* used a CNN to recognize wheat spikes and the accuracy was 95.91%. However, the time taken to complete each training was approximately 3 hours [28]. Wang *et al.* used full convolutional network (FCN) and Harris corner detection method [29] to segment and count wheat ears, respectively [30]. The segmentation model was trained by 4,550 training images and 1,950 verification images. The training time was over 10 hours [30].

So far, image processing has been developed and used to detect the disease infection of wheat ears or wheat ear counting [9]–[28], [30]–[33]. However, in the previous research only the severity of a single diseased wheat ear was studied by image processing technology [34], but not on counting the number of diseased wheat ears in a wheat ear group. Also, there still lacks an effective method that can determine the severity of diseased wheat ear groups. In addition, all the previous studies, evaluating the effects of fungicide applications on the control wheat FHB [35], [36], employ a manual assessment method by counting the number of wheat ears affected to determine the efficacy of fungicide application programs [37]. Such traditional disease severity assessment method is laborious and time-consuming.

To overcome these disadvantages, we used machine learning techniques from artificial intelligence, with the objectives of 1) proposing to combine K-means clustering algorithm and random forest classifier to segment wheat ears and FHB diseased areas from wheat images; 2) proposing and developing a width mutation counting algorithm to count the number of all wheat ears and the wheat ears diseased; and 3) rating the severity of FHB on wheat ear groups. The goal of this study was to develop a digital imaging method that could evaluate the control effects of common fungicides based on the severity of wheat ear groups under the field conditions.

This paper is outlined as follows: Section II describes the experimental site and the images acquired. Section III describes the methods of segmenting wheat ears and counting wheat ears. Section IV presents the experimental results for segmenting and counting wheat ears. Section V discusses the effectiveness of proposed methods. Finally, Section VI provides the conclusion of this study.

II. EXPERIMENTAL DATA AND INFORMATION

A. EXPERIMENTAL SITE

The experimental site was located in Anhui Academy of Agricultural Sciences, Hefei, Anhui, China (31°89'47.76'' latitude North, 117°25'23.17'' longitude East). Figure 1 shows the layout of the experimental site and design. The size of each small experimental area was 1.5 m × 1.5 m. Figure 1(b) shows 24 study groups sprayed by six different fungicides (corresponding to the 6 different colors in Figure 1(b)). Control group A contained three healthy

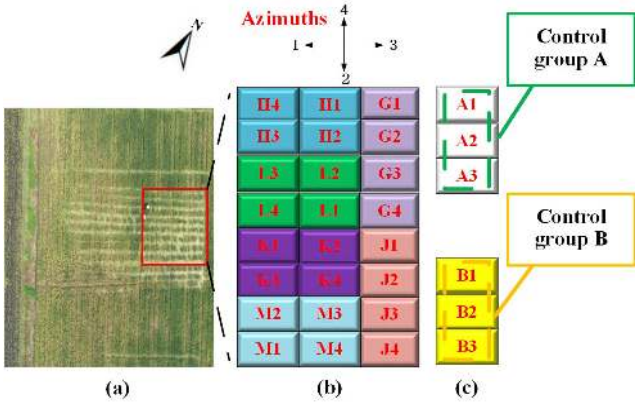

FIGURE 1. Experimental site layout and experimental design: (a) experimental site, (b) wheat ear groups sprayed by different fungicides, (c) control groups.

wheat ear groups. Control group B contained three wheat ear groups which were inoculated with *Fusarium graminearum* spore and sprayed with fungicides. A wheat ear group was selected in each color coded plot randomly. As shown in Figure 1(c), two wheat ear groups were selected for contrast at the areas of A1 and B1. Six wheat ear groups sprayed by six fungicides were selected for analysis at areas of G1, H1, J1, K1, L1 and M1. The six fungicides for the selected groups were commonly used in China [38]. The six study groups were sprayed with: 1) 50% Prochloraz [39] water emulsion (375mL/hm^2, 25μL), 2) 80% Tebuconazole [40] aqueous suspension concentrate (195mL/hm^2, 13μL), 3) 25% Pyraclostrobin [41] emulsifiable concentrate (300mL/hm^2, 20μL), 4) 50% JS399-19 [42] aqueous suspension concentrate (750mL/hm^2, 50μL), 5) 50% Carbendazim [43] wettable powders (750g/hm^2, 50mg), and 6) 30% Prothioconazole [44] dispersed oil suspension concentrate (360mL/hm^2, 24μL), respectively. Control group A was sprayed by water (600L/hm^2, 25ml). Control group B was sprayed by water (600L/hm^2, 25mL) after being inoculated the *F. graminearum* spore. The concentration of the spore for inoculation was 10^5/mL. The volumes of *F. graminearum* inoculation and fungicide application were all 25 mL in per wheat ear group of Figure 1(b).

All fungicide applications were made as standard recommendations [45], which met the national standard ''NY/T 1464.15-2007 Guidelines on efficacy evaluation of pesticides Part 15: Fungicides against fusarium head blight of wheat'' [46]. Readers can find the information of six fungicides retrieved from http://www.chinapesticide.org.cn/. The wheat cultivar used for the experiment was ''Huai-Mai-35''. The trial was planted on October 15,2018. The pathogen inoculation was made at the flowering stage on April 17, 2019. Fungicide applications were conducted on April 18, 2019. Fertilization and irrigation for the study followed local recommendations.

In Figure 2, there were four close-up instances of wheat ears. The color of wheat ears could become yellow or pink gradually when affected by FHB.

B. IMAGE COLLECTION

A Nikon D3200 digital camera was used to collect wheat images. With this camera each image had a size of 6,016 × 4,000 pixels. The viewing angle of photographing was 45°. The distance between the camera and the wheat ears was around 1.2 m. The aperture was f/3.5. The exposure time was 1/800s. The field of view was 0.8 m×0.8 m. The spatial resolution was 300 dpi×300 dpi. To avoid the interference from the background, such as wheat stalks, bare soil, weeds and light exposure, a non-reflective black fabric was used behind the wheat as image background. The black fabric also prevented the irrelevant wheat ears from being captured by the camera when photographing a wheat ear group. It also provided a unified background environment for further study based on hyperspectral images (it is necessary to provide a non-reflective black fabric to prevent over light exposure of the background when acquiring hyperspectral images) and experimental reproduction.

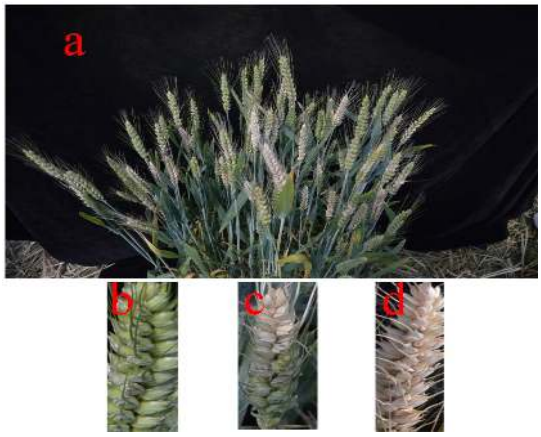

FIGURE 2. Close-up instances of wheat ears: (a) wheat ear group, (b) healthy wheat ear, (c) half healthy and half sill wheat ear, (d) sill wheat ear.

High-resolution digital images were collected during the filling stage of wheat. The images were collected from 9 a.m. to 3 p.m. on May 9, 2019. The weather of the day was sunny and windless. Choosing this time window was for the purpose of avoiding possible image inconsistency due to varying sun light and weather conditions. The reasons of choosing this plant growth stage to carry out the experiment were as follows: 1) wheat was just onset during the flowering stage and it was at the early stage of infection. There were not enough diseased wheat ears to show the disease level then. 2) The initial filling stage of wheat is an important window for secondary spraying. If the severity of disease can be accurately identified and diagnosed, it will be helpful to formulate effective control schemes and spray amount quantitatively, which may help reduce the amount of spraying pesticides to protect the environment. 3) When the wheat ears ripen, the color of diseased and healthy wheat ears are both yellow. It is difficult to distinguish them at that stage.

For each wheat ear group, four images were taken from four azimuths, which is shown by the numbers and arrows in the upper of Figure 1 (b). The four images from each wheat ear group were named as N_1, N_2, N_3, and N_4, where N represents the name of each wheat ear group.

III. METHODS

Figure 3 shows the flow chart of the relationship between the methods proposed and developed in this research, which included four parts: image transformation, image segmentation, wheat ear counting and spray application evaluation. The details of these methods were described in Section III-A to Section III-E.

A. IMAGE PREPROCESSING AND TRANSFORM

Image preprocessing included: 1) cropping the images of each wheat ear group entirely with a rectangular frame

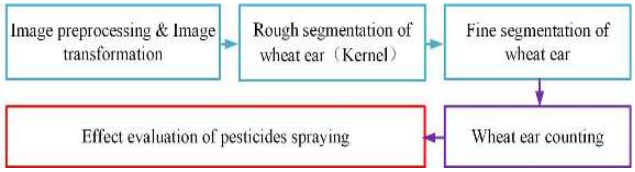

FIGURE 3. The flow chart of proposed and developed methods in this research.

to remove redundant background artifacts; 2) in order to improve the efficiency of the algorithm, resampling the size of each image uniformly to 2,000 × 2,000 pixels.

Image transform from a red-green-blue (RGB) image into a red-green-green (RGG) one was done by replacing the blue component in the RGB image with its green component after image enhancement. The image transform was for enlarging the gray-level value difference of wheat ear regions between RGB images and RGG images (Figure 11).

B. ROUGH SEGMENTATION ALGORITHM

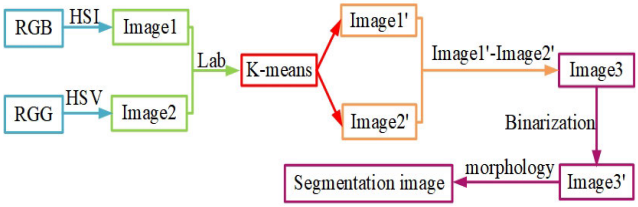

FIGURE 4. The flow chart of rough segmentation algorithm.

Figure 4 shows the process of rough segmentation. In this experiment, it was found that RGB images and RGG images had different colors in the regions of wheat ears after converting them to hue-saturation-intensity (HSI) color space and hue-saturation-value (HSV) color space, respectively. Therefore, firstly RGB images and RGG images were converted to HSI color space and HSV color space, respectively. Since the color gamut in lightness-a-b (Lab) color space is wider, it is beneficial for clustering. Therefore, all of the images were converted to Lab color space then. Figure 5 shows the clustering results for images that were converted or not converted to the Lab color space. Red circles in Figure 5(b) represent some regions having unsatisfactory clustering effect.

K-means algorithm is a common clustering algorithm and it divides the similar data points by presetting K value and the initial clustering center of each category [20]. The optimal clustering results are obtained by iterative optimization of the average distance between the divided cluster center and other points in the cluster [20]. According to the number of categories of main objects in each image and actual clustering result, K value was set as 4; The initial clustering center of each category was randomly sampled; The distance metric was set as Manhattan distance which represents the sum of the absolute wheelbase of two points on the standard coordinate system [47]. Three grayscale images of each image were respectively converted into one-dimensional column vectors,

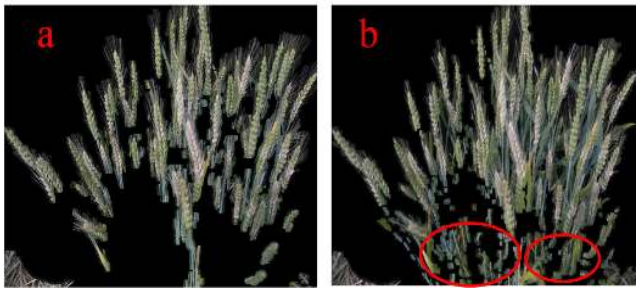

FIGURE 5. Comparison of clustering effect of a wheat ear group: (a) converted to Lab color space, (b) not converted to Lab color space.

and then merged them into a two-dimensional matrix. The two-dimensional matrix is the input variable of K-means algorithm.

Morphological operations of dilatation (structuring element: 'square', 2 × 2 pixels), deleting small area objects (threshold = 200, eight neighborhoods) and hole filling were used in the rough segmentation algorithm.

C. FINE SEGMENTATION ALGORITHM

After rough segmentation, most of leaves, stalks and wheat awns were removed. But still a part of leaves, stalks and wheat awns remained to be removed, which is the fine segmentation for.

For fine segmentation the random forest classifier and sliding window method were used to segment the rough images and diseased spots.

Random forest is an integrated algorithm that is built by a decision forest based on a decision tree learner [48]. Based on the training set resampling and voting mechanism, random attribute selection is introduced in the training process of random forest classifier [49]. Random forest has better generalization than a single decision tree classier and overcomes the shortcoming that the decision tree is easy to be over-fitting [50]. In view of the excellent classification and generalization ability, the random forest classifier was selected for fine segmentation of wheat ears and extraction of diseased spots in this research. The CART (classification and regression tree) decision algorithm was adopted in this paper. Twenty trees were set in the random forest classifier. Bootstrap aggregates for an ensemble of decision trees. TreeBagger (a function in MATLAB 2016a) bags an ensemble of decision trees for classification.

Morphological operations of dilatation (structuring element: 'square', 3 × 3 pixels), deleting small area objects (threshold = 200, eight neighborhoods) and hole filling were used in the fine segmentation algorithm.

1) TRAINING SAMPLES & SLIDING WINDOW SIZE

In training set, the numbers of wheat ear images and background images were 10 and 15, respectively. The background images included leaves, stalks, bare soils, lodging straws and wheat awns. Figure 6 is the examples of training set.

FIGURE 6. Examples of training set: (a) healthy wheat ear, (b) diseased wheat ear, (c) stalks, (d) leaves, (e) bare soils & lodging straws, (f) wheat awns.

If the sliding window is too large, the segmentation will perform poor; If the sliding window is too small, the training time will increase. According to the actual segmentation performance (see the part C of Section V), a 8 × 8-pixel window was determined to slide over the images of training set with a step of 8 pixels to obtain a total of 25,094 sub-images so that the training time was approximately 17 minutes.

2) FEATURE SELECTION

Eighteen features were selected from sample color, texture, and geometry, and vegetation index from images in the experiment.

a: COLOR FEATURES

Choosing six grayscale images extracted from the inputting image in RGB color space and Lab color space. Then, in order to enhance the difference between wheat ear regions and non-wheat ear regions, image 2D convolution operation was performed. The size of convolution kernel was 2 × 2 pixels. Figure 7 is the process of color feature extraction for image fine segmentation with random forest classifier.

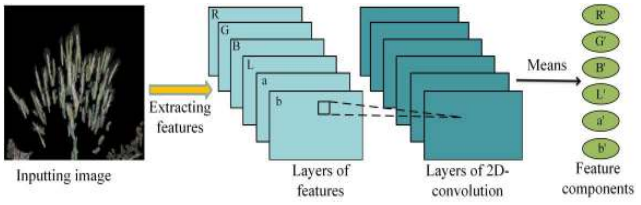

FIGURE 7. Process of extracting color features.

b: TEXTURE FEATURES

Choose four texture features generated by gray-level co-occurrence matrix (GLCM) [51]:

$$Contrast = \sum_{i,j} (i-j)^2 p_{ij} \quad (1)$$

$$Homogeneity = \sum_{i,j} p_{ij} \Big/ \left\lfloor 1 + (i-j)^2 \right\rfloor \quad (2)$$

$$Energy = \sum_{i,j} (p_{ij})^2 \quad (3)$$

$$Correlation = \left(\sum_{i,j} (i-\mu_x)(j-\mu_y) p_{ij} \right) \Big/ (\sigma_x \sigma_y) \quad (4)$$

where i is row, j is column, p_{ij} is the value of image in i row and j column, $\mu_x(\mu_y)$ is the mean of each image, $\sigma_x(\sigma_y)$ is standard deviation of each image.

The offset distance and angle of GLCM were set as 1 pixel and (−90°,0°,90°,180°), respectively. Other parameters were set as default.

c: VEGETATION INDEX FEATURES

It was found that the effect of image fine segmentation by combining normalized green-red difference vegetation index (NGRDI) and normalized green-blue difference vegetation index (NGBDI) is interesting to investigate. Therefore, a new vegetation index is proposed to integrate NGRDI and NGBDI into the normalized green-red-blue difference vegetation index (NGRBDI) as follows:

$$NGRBDI = (g-b)/(g+b) - \alpha(g-r)/(g+r) \quad (5)$$

where r=R/(R+G+B), g=G/(R+G+B), b=B/(R+G+B); R, G and B are the pixel values of three bands of the original image, respectively; "α" is an enhancement factor. In this experiment, the value of α was set as 2.

d: SHAPE INVARIANT MOMENT FEATURES

Hu [52] used central moment to construct seven invariant moments which can describe the region shape. These invariant moments have the characteristics of translation, scale, and rotation invariance. Therefore, invariant moments have become important regional feature sets and are widely used in the field of image detection [53], [54].

D. METHODS OF WHEAT EAR COUNTING

When photographing with an angle of inclination and a close distance, there were some sudden width changes happened in the heads, tails and mutual adhesions of connected domains of wheat ears. As shown in Figure 8, the reason why the width of wheat changed is that each wheat ear has a different angle and a jagged shape characteristic. In this paper, we only considered the case where the widths of connected domains of wheat ears were suddenly reduced or increased by more than 50% (see the width change of the red and blue lines in each green frame shown in Figure 8).

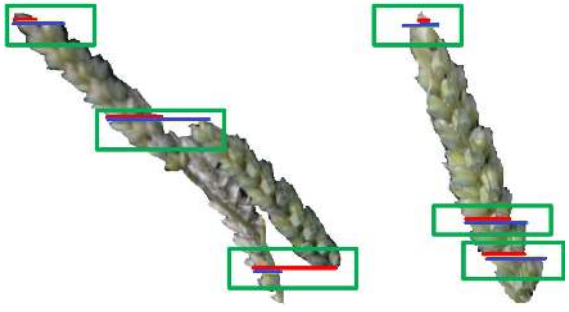

FIGURE 8. The width changes of wheat ears.

This phenomenon can be used to count wheat ears. And according to the place of width mutation, the problem of counting wheat ears with mutual occlusion can be resolved. The details are as follows:

1) METHOD OF COUNTING ALL WHEAT EARS

In this method, calculating the rate of width change between rows by scanning each connected domain row by row. Then finding the width mutation points by the rate of width change. At last, the number of wheat ears is calculated by the width mutation points. The pseudo-code of the width mutation algorithm is as follows:

The Pseudo-Code of the Width Mutation Algorithm

(i) Dividing connected domains of wheat ears. Acquiring the coordinates ($[x_{min},y_{min}]$, $[x_{max},y_{max}]$) in the top left corner and lower right corner of each connected domain, respectively. Calculating the height (H), width (W) and inclination angle (A0) of each connected domain. Calculating the average height (H0) of wheat ears in each image. The number of wheat ears (Count_A) is initially set as 0.
(ii) Three cases are divided: $H \leqslant H0$, $H0 < H \leqslant 2H0$, $2H0 < H$. The three cases have different threshold parameters: threshold_k, threshold_rate and threshold_width, which are (0.5, 0.5, W), (0.5, 0.4, W), (0.3, 0.3, W/2), respectively. The value of threshold_k and threshold_rate ranges from 0.3 to 0.5. According to the actual samples, the parameters can be adjusted. The second and third cases are for solving the problem of mutual occlusion.
(iii) In the third case, longitudinal division is performed at intervals of 2H0 at first. In the second and third cases, each connected domain is rotated to horizontal direction according to A0.
(iv) Scanning each connected domain row by row and calculate the rate of width change between row i and row i+1.
(v) if rate>threshold_rate, marking the rightmost points of row i and row i+1.
(vi) Marking the points ($[x_{min},y_{min}]$, $[x_{max},y_{max}]$). Removing the marked points that are too close to each other when the distance between them is less than 48.5 pixels.
(vii) Connecting all marked points to calculate slope-difference K between two neighboring lines. If K>threshold_k, Count_A plus one.
(viii) If there are only two marked points of each connected domain, Count_A plus one.
(ix) If H<H0/3 and W<threshold_weight, Count_A minus one.
(x) Outputting the number of wheat ears.

Figure 9 is the examples of the width mutation points and connection lines marked by the red circles and red lines, respectively. According to the above algorithm, when the slope-difference between two neighboring lines in Figure 9 is greater than the threshold_k, the number of wheat ears plus one. That is, the number of corners of lines (see the blue arcs in Figure 9) is equal to the number of wheat ears. According to actual observation, there are always corners between the mutual adhesions of wheat ears. Figure 9 shows the width mutation algorithm can detect the corners of mutual adhesions of wheat ears. So, the proposed counting method can solve the problem of mutual occlusion of wheat ears.

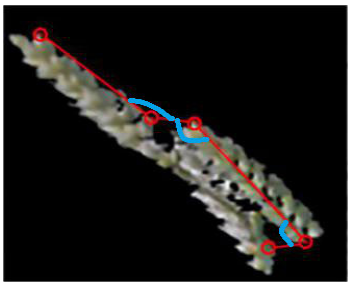

FIGURE 9. Width mutation points and lines.

2) METHOD OF COUNTING DISEASED WHEAT EARS

In this method, the regions of diseased spots need to be counted according to the connected domain. The pseudo-code is as follows:

The Pseudo-Code of Counting Diseased Wheat Ears

(i) Dividing connected domains of diseased spots.
(ii) Filtering out noise points with small area.
(iii) Calculating the average area (Area_A) of per connected domain.
(iv) The number of connected domains (Count_B) is initially set as 0. If the area of each connected domain is over than Area_A, the Count_B plus one.
(v) Outputting the number of diseased wheat ears (Count_B).

E. CRITERIA FOR EVALUATION ALGORITHM AND STANDARDS FOR FHB

According to national standard "GB/T 15796-2011 Rules for monitoring and forecast of the wheat head light" [55], the details of this standard are as follows:

1) SEVERITY OF SINGLE WHEAT EAR

The severity of individual wheat ears is catgorized into five levels (Table 1):

TABLE 1. Standard for evaluating severity of single wheat ear.

Area ratio between diseased spot and wheat ear (%, X)	level
0	0
X≤25	1
25<X≤50	2
50<X≤75	3
X≥75	4

The levels of diseased wheat ears measured in this experiment were greater than level 0.

2) RATE OF DISEASED WHEAT EARS

Calculating the rate of diseased wheat ears according to formula (6).

$$Y = \frac{number\ of\ diseased\ wheat\ ears}{number\ of\ all\ wheat\ ears} \times 100\% \quad (6)$$

3) CRITERIA FOR EVALUATION ALGORITHM

Four metrics, Pixel Accuracy (PA), Precision, Recall and F-measure, were used to evaluate segmentation quality [56]–[58]. PA and Precision represent the accuracy of the segmentation algorithm in all samples and positive samples, respectively. Recall represents the integrity of the segmentation image [30]. F-measure was used to balance Precision and Recall [30]. These metrics were calculated as follows:

$$PA = (\frac{TP + TN}{P + N}) \times 100\% \quad (7)$$

$$Precision = (\frac{TP}{TP + FP}) \times 100\% \quad (8)$$

$$Recall = (\frac{TP}{TP + FN}) \times 100\% \quad (9)$$

$$F - measure = (\frac{2 \times Precision \times Recall}{Precision + Recall}) \times 100\% \quad (10)$$

where TP represents the pixel area correctly predicted as wheat ear; TN represents the pixel area correctly predicted as background; FP is the pixel area predicted as wheat ear, but actually these pixels belong to the background. FN is the pixel area predicted as background, but actually these pixels belong to wheat ears. $P + N$ represents the sum pixel area of wheat ear and background in the manual field measurement.

The accuracy, R^2 (r-squared) and RMSE were used to evaluate the counting method [59]. The values of Accuracy and R^2 closer to 1 indicate better performance, as do smaller RMSE values.

$$Accuracy = \left(1 - \frac{|y_i - x_i|}{y_i}\right) \times 100\% \quad (11)$$

$$R^2 = 1 - \frac{\sum_1^N (y_i - x_i)^2}{\sum_1^N (y_i - \bar{y}_i)^2} \quad (12)$$

$$RMSE = \sqrt{\frac{\sum_1^N (y_i - x_i)^2}{N}} \quad (13)$$

where N is the number of test images, y_i is the actual number of wheat ears in image i, $\bar{y}_i$ is the actual average number of wheat ears per image, and x_i is the predicted number of wheat ears in image i.

IV. RESULTS

All data processing algorithms were programmed using MATLAB 2016a (MathWorks, Natick, Massachusetts, USA). The hardware used for implementation of the algorithms was a PC computer with Windows7/10 operating system, Intel(R) Core i7-3770 CPU processor and 8GB of memory.

A. IMAGE TRANSFORMATION

Figure 10 (a)&(b) are the examples of original RGB images and transformed RGG images, respectively. The result shows that the color visualization of the RGG image was changed compared with the original RGB image.

FIGURE 10. Comparison of image transformation: (a) a RGB image, (b) a RGG image.

B. ROUGH SEGMENTATION

Figure 11(a)&(b) are the clustering results of the images in Figure 10(a)&(b), respectively.

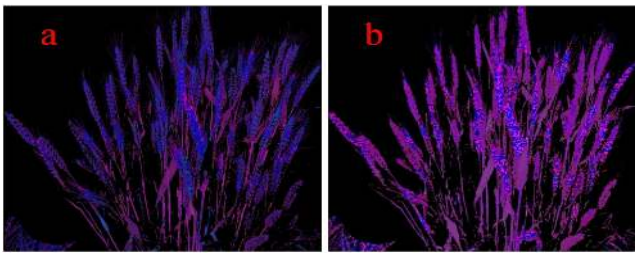

FIGURE 11. The clustering results of the RGB image and RGG image: (a) the clustering result of the RGB image, (b) the clustering result of the RGG image.

The colors of wheat ear regions were dark blue and purplish red in Figure 11(a)&(b), respectively. But the colors of leaves and stalks regions were purplish red in Figure 11(a)&(b). That is, the gray-level value difference of wheat ear regions between RGB images and RGG images is big. In order to remove leaves and stalks and extract wheat ears, the clustering result of the RGG image was subtracted from the clustering result of the RGB image. Figure 12 is the result of rough segmentation.

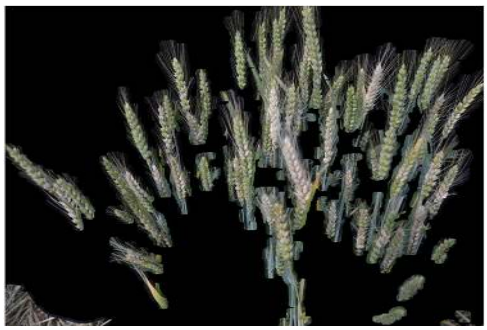

FIGURE 12. Result of rough segmentation.

C. FINE SEGMENTATION

Figure 13(a) is the fine segmentation result of a wheat ear group. After further fine segmentation, choosing regions of healthy wheat ears and diseased wheat ears as training set for segmenting diseased spots. Figure 13(b) is the result of diseased spots segmented.

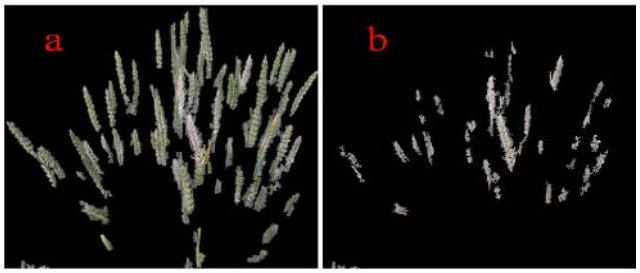

FIGURE 13. Final results of fine segmentation: (a) fine segmentation result of wheat ear group, (b) segmentation result of diseased spots.

D. COMPARISON OF WHEAT EAR SEGMENTATION PERFORMANCE

We compared the proposed segmentation method with three other segmentation methods, the Otsu method [60], the method of Liu *et al.* [17] and the method of Wang *et al.* [30], for wheat ear segmentation. The Otsu method and the method of Liu *et al.* are the traditional unsupervised segmentation methods. The method of Wang *et al.* is based on deep learning method of semantic segmentation (300 training images,100 verification images, learning rate = 0.001, batch size = 10, epochs = 30, and steps_per_epoch = 300). Figure 14 shows the segmentation results of these methods.

As shown in Figure 14, red circles represent the segmentation errors of each method, which indicate that the segmentation errors of the proposed method were less than other three methods. Many leaves, stalks and bare soils were not removed by using Otsu method. Some leaves or stalks were also not removed by using method of Liu *et al.* The error of the method of Wang *et al.* might be related to the neural network used, or the number of training data. To better evaluate the segmentation results, PA, Precision, Recall and F-measure were used to evaluate the segmentation effect of different segmentation method in Figure 15.

As shown in Figure 15, each color column and black line represent the mean and the standard deviation of four evaluating indicators of 32 testing images, respectively. The PA, Precision, Recall and F-measure of proposed method were 0.865, 0.518, 0.512, 0.511, respectively. In addition to the Recall indicator, the proposed method had a highest mean value in the other three indicators. Compared with Otsu method, there is more than a 17% improvement on average in the PA, Precision and F-measure; Compared with method of Liu *et al.*, there is more than a 16% improvement on average in Precision, Recall and F-measure; Compared with method of Wang *et al.*, there is more than a 2% and 7% improvement on average in PA and Precision evaluation index, respectively. In summary, the proposed segmentation method performs better than other three methods for segmenting wheat ears under the conditions of severe occlusion of wheat ears and little training samples.

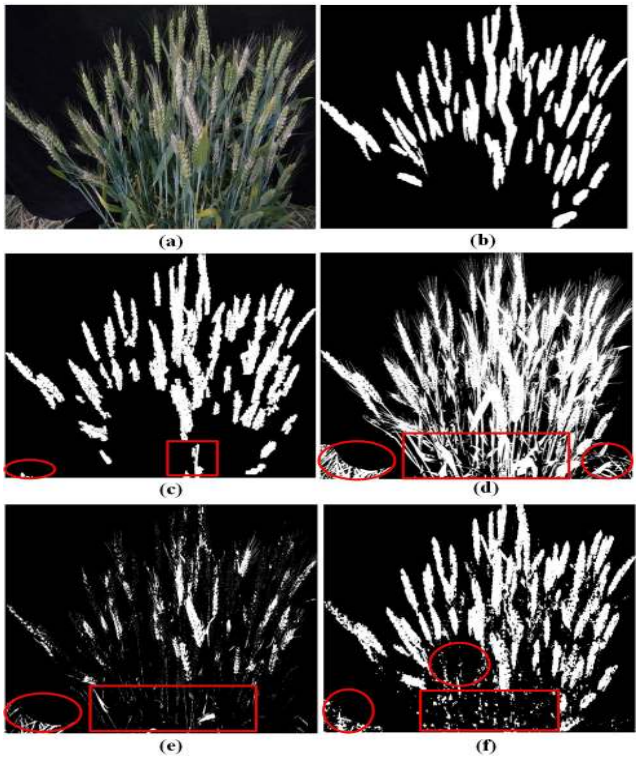

FIGURE 14. Comparison of different segmentation methods: (a) original image, (b) ground truth of original image, (c) segmentation result of newly proposed segmentation method, (d) segmentation result of Otsu method, (e) segmentation result of method of Liu *et al.*, (f) segmentation result of method of Wang *et al.*

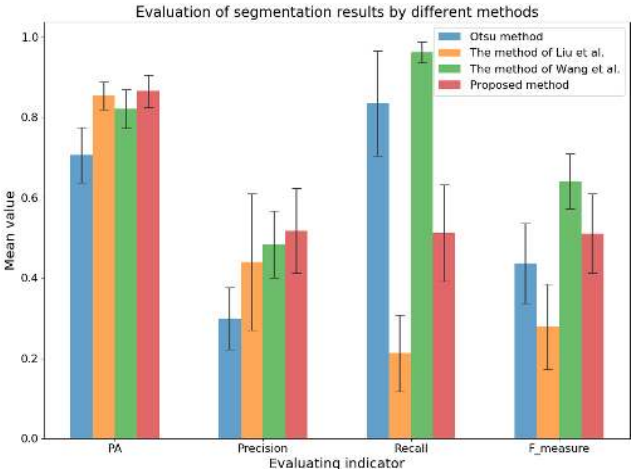

FIGURE 15. Evaluation of segmentation effects of different methods.

E. WHEAT EAR COUNTING AND CONTROL EFFECT EVALUATION OF PESTICIDE SPRAYING

Counting wheat ears whose occlusion rate was lower than 50% by manual visual method in the original images. For the reason of occlusion, the real numbers of wheat

TABLE 2. Results of counting all wheat ears in each image.

Image name	G1_1	G1_2	G1_3	G1_4	H1_1	H1_2	H1_3	H1_4	J1_1	J1_2	J1_3	J1_4
Proposed counting method	54	56	62	56	48	48	44	55	47	46	61	45
Measured value	61	60	67	61	51	47	49	48	53	50	62	49
Accuracy(%)	88.53	93.33	92.54	91.80	94.12	97.88	89.80	85.42	88.68	92.00	98.39	91.84
Harris corner detection method	53	54	75	72	57	57	55	60	63	45	71	54
Accuracy(%)	86.89	90.00	88.06	81.97	88.24	78.72	87.76	75.00	81.13	90.00	85.48	89.80
Image name	K1_1	K1_2	K1_3	K1_4	L2_1	L2_2	L2_3	L2_4	M3_1	M3_2	M3_3	M3_4
Proposed counting method	65	66	63	54	79	78	66	76	59	68	60	59
Measured value	71	70	68	58	80	79	68	78	60	65	64	63
Accuracy(%)	91.55	94.29	92.65	93.10	98.75	98.73	97.06	97.44	98.33	95.38	93.75	93.65
Harris corner detection method	87	58	81	63	72	72	62	82	65	70	81	68
Accuracy(%)	77.46	82.86	80.88	91.38	90.00	91.14	91.18	94.87	91.67	92.31	73.44	92.06

Image name	A1_1	A1_2	A1_3	A1_4	B1_1	B1_2	B1_3	B1_4
Proposed counting method	46	45	41	50	43	42	53	60
Measured value	51	48	45	56	52	48	50	59
Accuracy(%)	90.20	93.75	91.11	89.29	82.69	87.50	94.00	98.31
Harris corner detection method	45	44	40	63	62	55	55	52
Accuracy(%)	88.24	91.67	88.89	87.50	80.77	85.42	90.00	88.14

TABLE 3. Results of counting diseased wheat ears in each image.

Image name	G1_1	G1_2	G1_3	G1_4	H1_1	H1_2	H1_3	H1_4	J1_1	J1_2	J1_3	J1_4
Proposed counting method	32	36	40	30	26	24	24	24	23	22	38	26
Measured value	40	41	39	36	24	21	27	26	28	27	36	25
Accuracy(%)	80.00	87.80	97.44	83.33	91.67	85.71	88.89	92.31	82.14	81.48	94.44	96.00
Harris corner detection method	51	50	36	45	30	18	36	36	36	18	44	30
Accuracy(%)	72.50	78.05	92.31	75.00	75.00	85.71	66.70	61.54	71.43	66.67	77.78	80.00
Image name	K1_1	K1_2	K1_3	K1_4	L2_1	L2_2	L2_3	L2_4	M3_1	M3_2	M3_3	M3_4
Proposed counting method	24	16	32	22	74	55	56	66	11	19	15	24
Measured value	25	18	32	23	70	56	59	69	12	20	17	23
Accuracy(%)	96.00	88.89	100	95.65	94.29	98.21	94.92	95.65	91.67	95.00	88.24	95.65
Harris corner detection method	27	22	36	27	66	54	68	72	14	18	20	27
Accuracy(%)	92.00	77.78	87.50	82.61	94.29	96.43	84.75	95.65	75.00	90.00	82.35	82.61

Image name	A1_1	A1_2	A1_3	A1_4	B1_1	B1_2	B1_3	B1_4
Proposed counting method	0	1	2	0	41	40	45	47
Measured value	0	1	2	0	44	44	42	51
Accuracy(%)	—	100	100	—	93.18	90.91	92.86	92.16
Harris corner detection method	0	2	3	0	40	37	50	45
Accuracy(%)	—	50.00	50.00	—	90.91	84.09	80.95	88.24

ears of each image pictured in different azimuth were different. Table 2 and Table 3 shows the results of wheat ear counting.

To evaluate the proposed counting method, we compared the proposed counting method with the Harris corner detection method which used by Liu *et al.* and Wang *et al.* Table 2 shows that the highest accuracy of proposed counting method was 98.39%, the lowest accuracy was 82.86%. Table 3 shows that the highest accuracy of proposed counting method was 100%, lowest accuracy was 80%. The difference between the predicted value and the measured value of proposed counting method was no more than 10. And the counting accuracy of proposed counting method exceeded that of the Harris corner detection method.

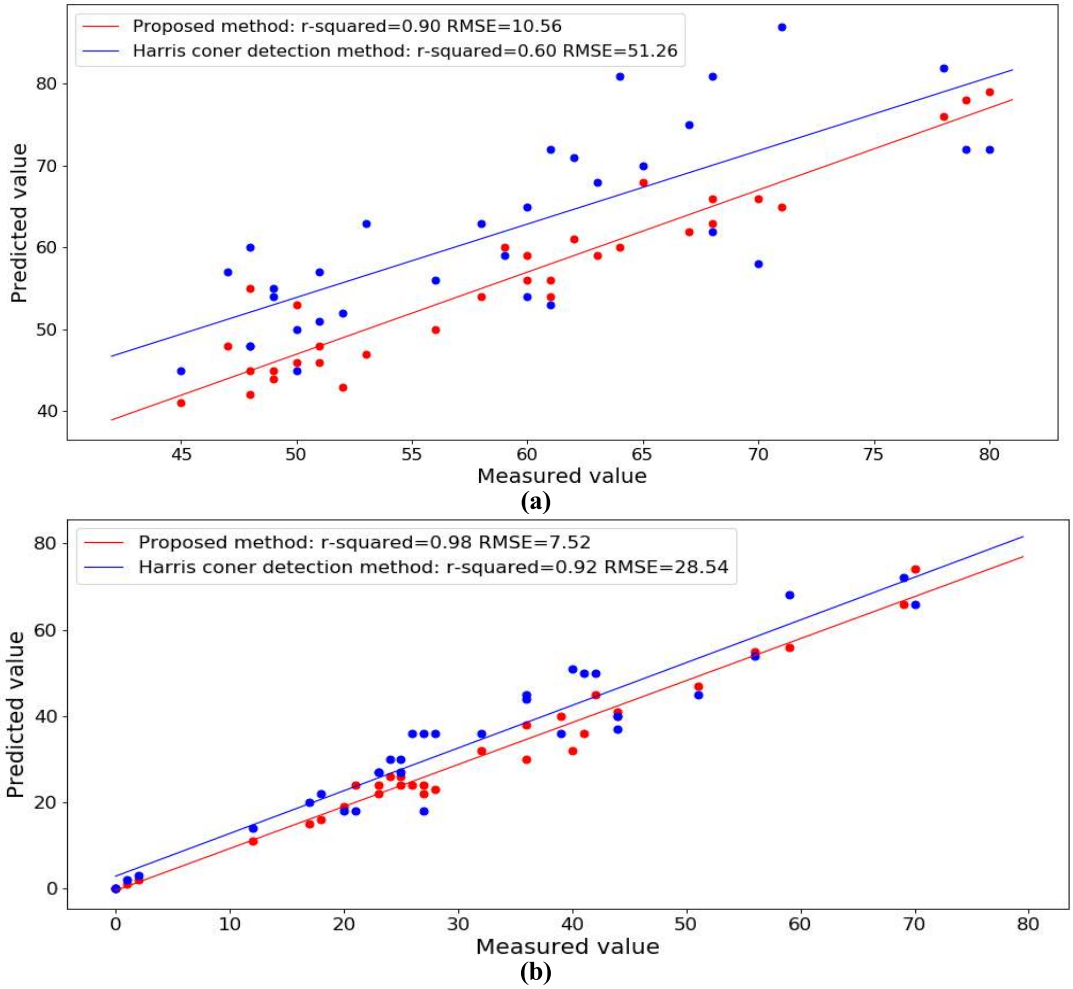

FIGURE 16. Fitting between predicted value and measured value: (a) fitting result of all wheat ears, (b) fitting result of diseased wheat ears.

In Figure 16(a), R^2 of proposed counting method and Harris corner detection method were 0.90 and 0.60, respectively. RMSE were 10.56 and 51.26, respectively. In Figure 16(b), R^2 were 0.98 and 0.92, respectively; RMSE were 7.52 and 28.54, respectively. Figure 16 shows that the predicted value of all wheat ears and diseased wheat ears were highly correlated with the measured value of ones by proposed counting method.

According to the standard in Section III-E, Table 4 shows that: (1) the difference value between predicted average Y and measured average Y was less than 4% in each wheat ear group; (2) according to measured average Y and actual disease index between B1 and other wheat ear groups, six pesticides all had a control effect of FHB; (3) the higher rate of diseased wheat ears, the worse control effect evaluation of pesticide spraying was. According to the value of predicted average Y, the relationship of selected wheat ear groups was:B1>L1>G1>J1>H1>K1>M1>A1. That is, the predicted control efficacy of six fungicides was: Prothioconazole > JS399-19 > Tebuconazole > Pyraclostrobin > Prochloraz > Carbendazim.

According to manual statistics of plant protection experts in Table 4, the actual disease index relationship of selected wheat ear groups was: B1>L1>G1>J1>H1>K1>M1>A1. Actual control effect relationship of the six fungicides is: Prothioconazole > JS399-19 > Tebuconazole > Pyraclostrobin > Prochloraz > Carbendazim. It means that the actual control effect relationship of the six fungicides is consistent with the relationship predicted by theproposed counting method.

V. DISCUSSION

A. COMPARISON OF THE SEGMENTATION EFFECT OF NGRBDI

As shown in Figure 17, there are the segmentation results of NGBDI, NGRBDI, NGRDI and VDVI (visible band difference vegetation index). Comparing these red circles and green circles, it is found that NGRBDI can better segment wheat ears and remove leaves or stalks than other vegetation indices.

To better evaluate the segmentation results, PA, Precision, Recall and F-measure were used to evaluate the segmentation effect of the proposed vegetation index. As shown

TABLE 4. Control efficacy evaluation of fungicide spraying.

Image name	G1_1	G1_2	G1_3	G1_4	H1_1	H1_2	H1_3	H1_4	J1_1	J1_2	J1_3	J1_4
Predicted Y(%)	60.38	72.00	64.52	54.55	54.17	50.00	54.55	43.64	55.32	55.00	62.30	57.78
Measured Y(%)	65.57	68.33	58.21	59.02	48.00	44.68	55.10	54.17	52.83	54.00	58.06	51.02
Predicted average Y(%)	62.86				50.59				57.60			
Measured average Y(%)	61.96				50.49				53.98			
Fungicide name	50% Prochloraz				80% Tebuconazole				25% Pyraclostrobin			
Actual disease index	16.88				9.25				15.13			
Actual control efficacy	68.06				82.49				71.37			
Image name	K1_1	K1_2	K1_3	K1_4	L2_1	L2_2	L2_3	L2_4	M3_1	M3_2	M3_3	M3_4
Predicted Y(%)	38.46	24.20	50.79	40.74	93.67	70.51	84.85	86.84	18.64	27.94	25.42	40.67
Measured Y(%)	35.21	25.71	47.06	38.33	87.50	70.89	86.76	88.46	20.00	30.77	27.42	37.70
Predicted average Y(%)	38.55				83.97				28.17			
Measured average Y(%)	36.58				83.40				28.97			
Fungicide name	50% JS399-19				50% Carbendazim				30% Prothioconazole			
Actual disease index	6.13				26.00				4.38			
Actual control effect(%)	88.41				50.79				91.72			
Image name	A1_1	A1_2	A1_3	A1_4	B1_1	B1_2	B1_3	B1_4				
Predicted Y(%)	0	2.01	4.44	0	93.18	95.24	84.91	73.43				
Measured Y(%)	0	2.01	4.44	0	88.00	91.67	84.00	86.44				
Predicted average Y(%)	1.61				86.69							
Measured average Y(%)	1.61				87.53							
Actual disease index	0.75				52.83							

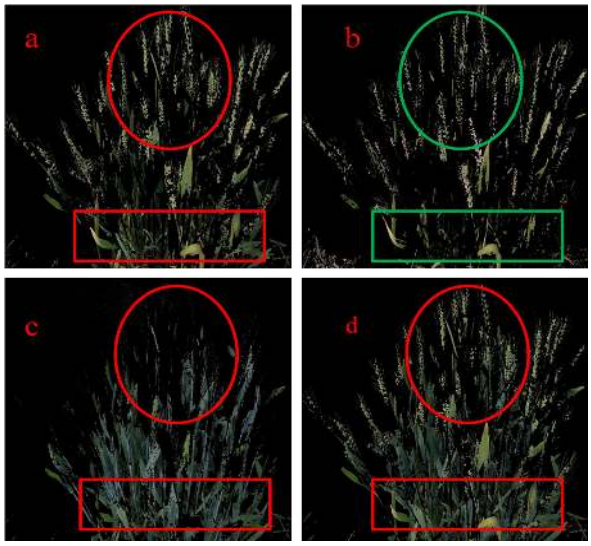

FIGURE 17. Segmentation results of different vegetation indices: (a) NGBDI, (b) NGRBDI, (c) NGRDI, (d) VDVI.

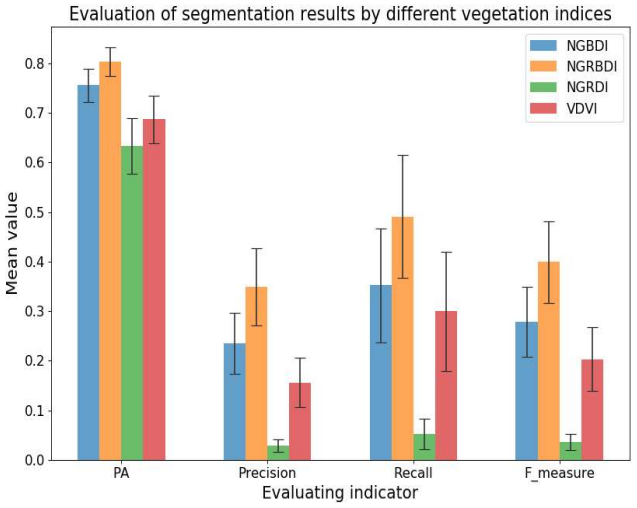

FIGURE 18. Evaluation of the segmentation effects of different vegetation indices.

in Figure 18, the proposed vegetation index had a highest mean value in each evaluation indicator. And compared with NGBDI, NGRDI and VDVI, NGRBDI was more than a 6% improvement in each evaluation index. Therefore, the newly proposed vegetation index (NGRBDI) is suitable for wheat ears segmentation in this research.

B. THE VISUALLY COMPARISON BETWEEN THE PROPOSED WIDTH MUTATION COUNTING METHOD AND HARRIS CORNER DETECTION METHOD

Figure 19 visually shows the difference between the proposed width mutation counting method and the Harris corner detection method. As shown in Figure 19(a), three images represent a single wheat ear, two adhered wheat ears and three adhered wheat ears, respectively. As shown in Figure 19(b), the red circles represent the width mutation points. The number of blue arcs represents the number of wheat ears predicted by proposed counting method. In Figure 19(c), the blue points represent the Harris corner points of each wheat-ear skeleton, which is done by scanning the binary wheat-ear images. Because of the rough boundary of each binary wheat-ear image, there are many corners of each wheat-ear skeleton. Thus, the number of Harris corner points increased so that the counting error greatly increased.

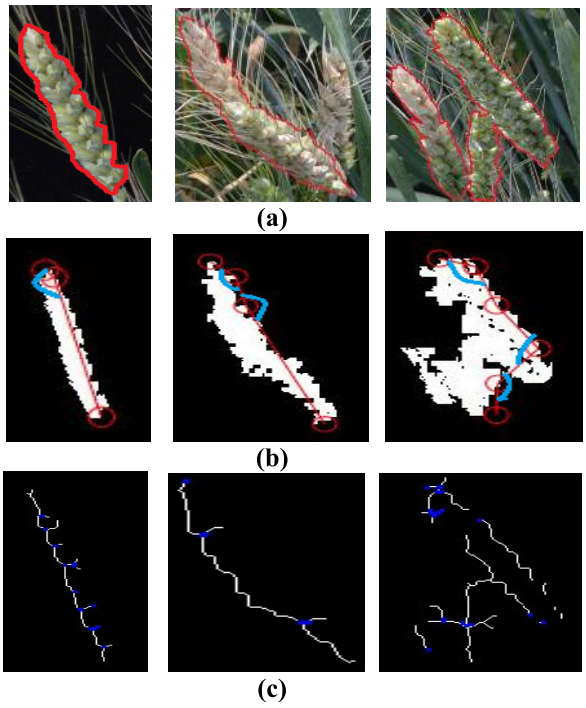

FIGURE 19. Comparison of different counting methods: (a) wheat ears in original images, (b) result of the proposed counting method, (c) result of Harris corner.

The comparison with the Harris corner detection method illustrates that the proposed counting method is more accurate when counting wheat ears and has better performance in solving the mutual occasion problem of wheat ears.

C. ANALYSIS OF THE SIZE OF SLIDING WINDOW AND IMAGE RESOLUTION

To study the impact of the size of the sliding window, we used 20 2,000 × 2.000 pixel images to analyze the change of the segmentation accuracy. As shown in Figure 20, the mean value of each indicator increased significantly when the size of the sliding window decreased from 14 × 14-pixel to 8 × 8-pixel. The mean value of each indicator changed a little when the size of the sliding window decreased from 8 × 8-pixel to 4 × 4-pixel. In addition, the number of training samples and training time increased when the size of the sliding window decreased. The conclusion is that the size of the sliding window is reasonable at 8 × 8-pixel.

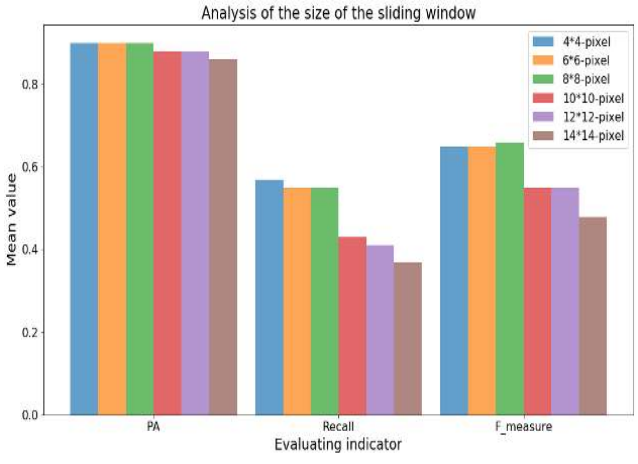

FIGURE 20. Analysis of the size of the sliding window.

We analyzed the segmentation results by different image resolution. In order to eliminate the effect of sliding window, the size of the sliding window was set as 8 × 8-pixel in each image resolution. As shown in Figure 21, the mean value decreased when the resolution of each image decreased from 1,500 × 1,500-pixel to 500 × 500-pixel in Recall and F-measure. The mean value of each evaluation indicator changed a little from 2,500 × 2,500-pixel to 1,500 × 1,500-pixel. However, the training time increased when the image resolution increased. Therefore, the 2,000 × 2,000-pixel was reasonably set in this experiment.

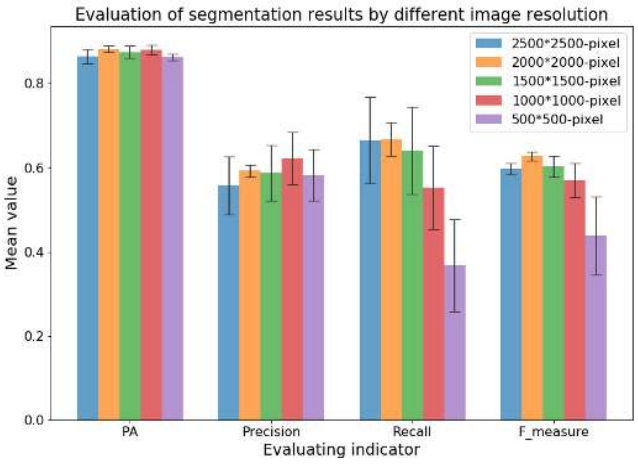

FIGURE 21. Analysis of the resolution of original images.

D. EFFECTS OF DIFFERENT BRIGHTNESS CONDITIONS

The formula used to calculate brightness of each original image is as follow:

$$Brightness = 0.229 \times r + 0.587 \times g + 0.114 \times b \quad (14)$$

where r, g and b are the mean of each band in RGB image. Figure 22 shows the change of brightness in the 24 images.

The method of Zhou *et al.* [21] is sensitive to illumination. According to Figure 22, different images taken from four azimuths have different average brightness. However, the errors between the predicted value and the measured value shown in Table 2 and Table 3 are not significant. That means the proposed algorithm is robust to different brightness conditions, and camera aperture is adjustable. Therefore, the effect of illumination in this experiment is small. However, in order to ensure the accuracy of wheat ear counting and image segmentation, it is recommended to collect image data in sunny and windless weather.

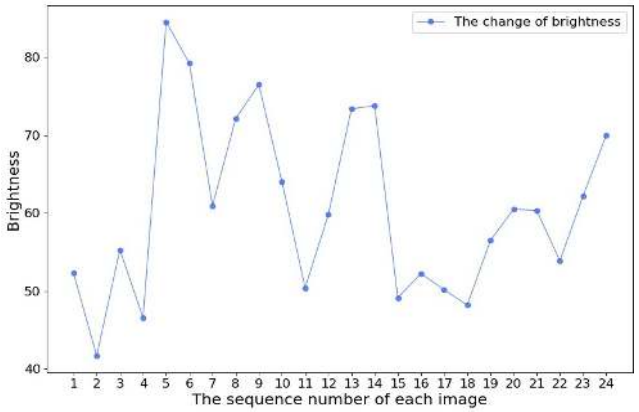

FIGURE 22. Brightness of three wheat ear groups.

VI. CONCLUSION

In this paper, a proposed algorithm based on image transformation and K-means clustering was used for rough segmentation and combining random forest classifier for fine segmentation. Selecting 18 features in the experiment to improve the effect of fine segmentation and a new vegetation index (NGRBDI) was created. Furthermore, the width mutation counting algorithms improved the average counting accuracy of all wheat ears and diseased wheat ears. Finally, the predicted relationship of control efficacy evaluation of fungicides is completely consistent with the actual control efficacy relationship rated by plant protection specialists.

The results of this research show that the proposed algorithm can correctly evaluate the efficacy of fungicides for controlling the wheat FHB disease under the field conditions. However, considering that effect of wheat ear counting depends on accuracy of image segmentation, further investigations are needed to verify whether the proposed segmentation method is suitable under other more complex field conditions. Further research is also needed to study the effects of different application rates of fungicides on control efficacy.

ACKNOWLEDGMENT

D. Zhang and Y. Chen designed this field experiment and revised this article; Z. Wang analyzed data and drafted this article; Y. Huang corrected this article and provided opinions and suggestions to improve the research; and N. Jin and C. Gu reviewed this article.

REFERENCES

[1] P. R. Shewry, "Wheat," *J. Exp. Botany*, vol. 60, no. 6, pp. 1537–1553, Apr. 2009.

[2] M. Figueroa, K. E. Hammond-Kosack, and P. S. Solomon, "A review of wheat diseases–A field perspective," *Mol. Plant Pathol.*, vol. 19, no. 6, pp. 1523–1536, Jun. 2018.

[3] B. Shiferaw, M. Smale, H.-J. Braun, E. Duveiller, M. Reynolds, and G. Muricho, "Crops that feed the world 10. Past successes and future challenges to the role played by wheat in global food security," *Food Secur.*, vol. 5, no. 3, pp. 291–317, Jun. 2013.

[4] J. K. Haile, A. N'Diaye, S. Walkowiak, K. T. Nilsen, J. M. Clarke, H. R. Kutcher, B. Steiner, H. Buerstmayr, and C. J. Pozniak, "Fusarium head blight in durum wheat: Recent status, breeding directions, and future research prospects," *Phytopathology*, vol. 109, no. 10, pp. 1664–1675, Oct. 2019.

[5] F. A. M. Saccon, D. Parcey, J. Paliwal, and S. S. Sherif, "Assessment of fusarium and deoxynivalenol using optical methods," *Food Bioprocess Technol.*, vol. 10, no. 1, pp. 34–50, Jan. 2017.

[6] M. Mcmullen, G. Bergstrom, E. De Wolf, R. Dill-Macky, D. Hershman, G. Shaner, and D. Van Sanford, "A unified effort to fight an enemy of wheat and barley: Fusarium head blight," *Plant Disease*, vol. 96, no. 12, pp. 1712–1728, Dec. 2012.

[7] M. Cuperlovic-Culf, L. Wang, L. Forseille, K. Boyle, N. Merkley, I. Burton, and P. R. Fobert, "Metabolic biomarker panels of response to fusarium head blight infection in different wheat varieties," *PLoS ONE*, vol. 11, no. 4, Apr. 2016, Art. no. e0153642, doi: 10.1371/journal.pone.0153642.

[8] X. Cheng, G. Qiu, J. Hu, W. Wu, Y. Chen, Y. Zhao, and T. Huang, "Control efficiency of different pesticides and application technologies against wheat scab," *J. Agricult.*, vol. 6, no. 1, pp. 28–32, 2016.

[9] A. Johannes, A. Picon, A. Alvarez-Gila, J. Echazarra, S. Rodriguez-Vaamonde, A. D. Navajas, and A. Ortiz-Barredo, "Automatic plant disease diagnosis using mobile capture devices, applied on a wheat use case," *Comput. Electron. Agricult.*, vol. 138, pp. 200–209, Jun. 2017.

[10] H. M. Khaeim, A. Clark, T. Pearson, and D. D. Van Sanford, "Methods of assessing fusarium damage to wheat kernels," *Al-Qadisiyah J. Agricult. Sci. (QJAS) (P-ISSN:E-ISSN)*, vol. 9, no. 2, pp. 297–308, Dec. 2019.

[11] S. D. Khirade and A. B. Patil, "Plant disease detection using image processing," in *Proc. Int. Conf. Comput. Commun. Control Autom.*, Feb. 2015, pp. 768–771.

[12] E. Hamuda, M. Glavin, and E. Jones, "A survey of image processing techniques for plant extraction and segmentation in the field," *Comput. Electron. Agricult.*, vol. 125, pp. 184–199, Jul. 2016.

[13] J. G. A. Barbedo, L. V. Koenigkan, and T. T. Santos, "Identifying multiple plant diseases using digital image processing," *Biosyst. Eng.*, vol. 147, pp. 104–116, Jul. 2016.

[14] A. Paul, S. Ghosh, A. K. Das, S. Goswami, S. D. Choudhury, and S. Sen, "A review on agricultural advancement based on computer vision and machine learning," *Emerg. Technol. Model. Graph.*, vol. 937, pp. 567–581, Jul. 2019.

[15] J. A. Fernandez-Gallego, S. C. Kefauver, N. A. Gutiérrez, M. T. Nieto-Taladriz, and J. L. Araus, "Wheat ear counting in-field conditions: High throughput and low-cost approach using RGB images," *Plant Methods*, vol. 14, no. 1, pp. 1–12, Mar. 2018.

[16] F. Cointault and P. Gouton, "Texture or color analysis in agronomic images for wheat ear counting," in *Proc. 3rd Int. IEEE Conf. Signal-Image Technol. Internet-Based Syst.*, Dec. 2007, pp. 696–701.

[17] T. Liu, C. Sun, L. Wang, X. Zhong, X. Zhu, and W. Guo, "In-field wheatear counting based on image processing technology," *Trans. Chin. Soc. Agricult. Machinery*, vol. 45, no. 2, pp. 282–290, 2014.

[18] M. Fan, Q. Ma, J. Liu, Q. Wang, Y. Wang, and X. Duan, "Counting method of wheatear in field based on machine vision technology," *Trans. Chin. Soc. Agricult. Machinery*, vol. 46, pp. 234–239, May 2015.

[19] F. Zhao, K. Wang, and Y. Yuan, "Study on wheat spike identification based on color features and adaboost algorithm," *Crops*, vol. 34, no. 1, pp. 140–145, Jan. 2014.

[20] Z. Liu, W. Huang, and L. Wang, "Field wheat ear counting automatically based on improved K-means clustering algorithm," *Trans. Chin. Soc. Agricult. Eng. (Trans. CSAE)*, vol. 35, no. 3, pp. 174–181, 2019.

[21] C. Zhou, D. Liang, X. Yang, B. Xu, and G. Yang, "Recognition of wheat spike from field based phenotype platform using multi-sensor fusion and improved maximum entropy segmentation algorithms," *Remote Sens.*, vol. 10, no. 2, p. 246, Feb. 2018.

[22] H. Ma, W. Huang, Y. Jing, S. Pignatti, G. Laneve, Y. Dong, H. Ye, L. Liu, A. Guo, and J. Jiang, "Identification of fusarium head blight in winter wheat ears using continuous wavelet analysis," *Sensors*, vol. 20, no. 1, p. 20, Dec. 2019.

[23] J. Ma, Y. Li, K. Du, F. Zheng, L. Zhang, Z. Gong, and W. Jiao, "Segmenting ears of winter wheat at flowering stage using digital images and deep learning," *Comput. Electron. Agricult.*, vol. 168, Jan. 2020, Art. no. 105159.

[24] A. Kamilaris and F. X. Prenafeta-Boldú, "Deep learning in agriculture: A survey," *Comput. Electron. Agricult.*, vol. 147, pp. 70–90, Apr. 2018.
[25] H. Yu, Z. Yang, L. Tan, Y. Wang, W. Sun, M. Sun, and Y. Tang, "Methods and datasets on semantic segmentation: A review," *Neurocomputing*, vol. 304, pp. 82–103, Aug. 2018.
[26] L. Zhang, Y. Chen, Y. Li, J. Ma, and K. Du, "Detection and Counting System for winter wheat ears based on convolutional neural network," *Trans. Chin. Soc. Agricult. Machinery*, vol. 50, no. 3, pp. 144–150, 2019.
[27] P. Sadeghi-Tehran, N. Virlet, E. M. Ampe, P. Reyns, and M. J. Hawkesford, "DeepCount: In-field automatic quantification of wheat spikes using simple linear iterative clustering and deep convolutional neural networks," *Frontiers Plant Sci.*, vol. 10, p. 1176, Sep. 2019.
[28] M. P. Pound, J. A. Atkinson, D. M. Wells, T. P. Pridmore, and A. P. French, "Deep learning for multi-task plant phenotyping," in *Proc. IEEE Int. Conf. Comput. Vis. Workshops (ICCVW)*, Oct. 2017, pp. 2055–2063.
[29] P. Ram and S. Padmavathi, "Analysis of Harris corner detection for color images," in *Proc. Int. Conf. Signal Process., Commun., Power Embedded Syst. (SCOPES)*, Oct. 2017, pp. 405–410.
[30] D. Wang, Y. Fu, G. Yang, X. Yang, D. Liang, C. Zhou, N. Zhang, H. Wu, and D. Zhang, "Combined use of FCN and harris corner detection for counting wheat ears in field conditions," *IEEE Access*, vol. 7, pp. 178930–178941, 2019.
[31] X. Jin, L. Jie, S. Wang, H. Qi, and S. Li, "Classifying wheat hyperspectral pixels of healthy heads and Fusarium head blight disease using a deep neural network in the wild field," *Remote Sens.*, vol. 10, no. 3, p. 395, 2018.
[32] L. Huang, Z. Wu, W. Huang, H. Ma, and J. Zhao, "Identification of Fusarium head blight in winter wheat ears based on Fisher's linear discriminant analysis and a support vector machine," *Appl. Sci.*, vol. 9, no. 18, p. 3894, Sep. 2019.
[33] Y. Yanjun, Z. Yulin, T. Qingjiu, W. Lei, W. Peiyan, and Z. Wenmin, "Winter wheat extraction using curvilinear integral of GF-1 NDVI time series," in *Proc. IEEE Int. Geosci. Remote Sens. Symp. (IGARSS)*, Jul. 2016, pp. 3174–3177.
[34] D. Zhang, D. Wang, S. Du, L. Huang, H. Zhao, D. Liang, C. Gu, and X. Yang, "A rapidly diagnosis and application system of fusarium head blight based on smartphone," in *Proc. 8th Int. Conf. Agro-Geoinformatics (Agro-Geoinformatics)*, Istanbul, Turkey, Jul. 2019, pp. 1–5.
[35] H. Lin, B. Dong, and J. Hu, "Residue and intake risk assessment of prothioconazole and its metabolite prothioconazole-desthio in wheat field," *Environ. Monitor. Assessment*, vol. 189, no. 5, p. 236, Apr. 2017.
[36] P. A. Paul, J. D. Salgado, G. Bergstrom, C. A. Bradley, "Integrated effects of genetic resistance and prothioconazole+ tebuconazole application timing on Fusarium head blight in wheat," *Plant Disease*, vol. 103, no. 2, pp. 223–237, Feb. 2019.
[37] C. Cowger, C. Arellano, D. Marshall, and J. Fitzgerald, "Managing fusarium head blight in winter barley with cultivar resistance and fungicide," *Plant Disease*, vol. 103, no. 8, pp. 1858–1864, Aug. 2019.
[38] Y. Chen, J. Wang, R. Yang, and Z. Ma, "Current situation and management strategiesof Fusarium head blight in China," *Plant Protection*, vol. 43, no. 5, pp. 11–17, 2017.
[39] T. Zhang, Q. Cao, N. Li, D. Liu, and Y. Yuan, "Transcriptome analysis of fungicide-responsive gene expression profiles in two penicillium italicum strains with different response to the sterol demethylation inhibitor (DMI) fungicide prochloraz," *BMC Genomics*, vol. 21, no. 1, Feb. 2020.
[40] S. A. Omer and N. A. Fakhre, "Simultaneous determination of ternary mixture of carboxin, chlorpyrifos, and tebuconazole residues in cabbage samples using three spectrophotometric methods," *J. Anal. Methods Chem.*, vol. 2020, pp. 1–16, Feb. 2020.
[41] Y. Y. Gao, X. X. Li, L. F. He, B. X. Li, W. Mu, and F. Liu, "Effect of application rate and timing on residual efficacy of pyraclostrobin in the control of pepper anthracnose," *Plant Disease*, vol. 104, no. 3, pp. 958–966, Mar. 2020.
[42] R. D. Wollenberg, S. S. Donau, T. T. Nielsen, J. L. Sørensen, H. Giese, R. Wimmer, and T. E. Søndergaard, "Real-time imaging of the growth-inhibitory effect of JS399-19 on Fusarium," *Pesticide Biochem. Physiol.*, vol. 134, pp. 24–30, Nov. 2016.
[43] H. Chen, Q. Wu, G. Zhang, J. Wu, F. Zhu, H. Yang, and Y. Zhuang, "Carbendazim-resistance of Gibberella Zeae associated with fusarium head blight and its management in Jiangsu Province, China," *Crop Protection*, vol. 124, Oct. 2019, Art. no. 104866.
[44] K. Hudec, J. Ki inová, and M. Mihók, "Changes of species spectrum associated with fusarium head blight caused by fungicides," *J. Central Eur. Agricult.*, vol. 20, no. 1, pp. 376–388, 2019.
[45] H. Wang, Y. Guo, C. Mu, Q. Wang, L. Bao, Y. Ma, W. Chen, W. Hou, and X. Gao, "Control effects of different fungicides against wheat sharp eyespot and wheat scab," *Plant Protection*, vol. 43, no. 1, pp. 193–198, 2017.
[46] *Guidelines on Efficacy Evaluation of Pesticides Part 15: Fungicides Against Fusarium Head Blight of Wheat*, NY/T 1464.15-2007, The ministry of agriculture of the People's Republic of China, Beijing, China, 2007.
[47] H. Kashima, J. Hu, B. Ray, and M. Singh, "K-means clustering of proportional data using l1 distance," in *Proc. 19th Int. Conf. Pattern Recognit.*, Dec. 2008, pp. 1–4.
[48] L. Breiman, "Random forests," *Mach. Learn.*, vol. 45, no. 1, pp. 5–32, Oct. 2001.
[49] J. Elith, J. R. Leathwick, and T. Hastie, "A working guide to boosted regression trees," *J. Animal Ecology*, vol. 77, no. 4, pp. 802–813, Jul. 2008.
[50] Z. Zhou, "Ensemble learning," in *Machine Learning*, Beijing, China: Tsinghua Univ. Press, 2016, pp. 171–178.
[51] R. Usha and K. Perumal, "SVM classification of brain images from MRI scans using morphological transformation and GLCM texture features," *Int. J. Comput. Syst. Eng.*, vol. 5, no. 1, pp. 18–23, Jan. 2019.
[52] M.-K. Hu, "Visual pattern recognition by moment invariants," *IEEE Trans. Inf. Theory*, vol. 8, no. 2, pp. 179–187, Feb. 1962.
[53] R. S. Siqueira, G. R. Alexandre, J. M. Soares, and G. A. P. The, "Triaxial slicing for 3-D face recognition from adapted rotational invariants spatial moments and minimal keypoints dependence," *IEEE Robot. Autom. Lett.*, vol. 3, no. 4, pp. 3513–3520, Oct. 2018.
[54] H. Mu and D. Qi, "Pattern recognition of wood defects types based on Hu invariant moments," in *Proc. 2nd Int. Congr. Image Signal Process.*, Oct. 2009, pp. 1–5.
[55] *Rules for Monitoring and Forecast of the Wheat Head Light*, GB/T 15796-2011, General Administration of Quality Supervision, Inspection and Quarantine of the People's Republic of China, Beijing, China, 2011.
[56] X. Xiong, L. Duan, L. Liu, H. Tu, P. Yang, D. Wu, G. Chen, L. Xiong, W. Yang, and Q. Liu, "Panicle-SEG: A robust image segmentation method for rice panicles in the field based on deep learning and superpixel optimization," *Plant Methods*, vol. 13, no. 1, p. 104, Nov. 2017.
[57] B. Ma, Z. Liu, F. Jiang, Y. Yan, J. Yuan, and S. Bu, "Vehicle detection in aerial images using rotation-invariant cascaded forest," *IEEE Access*, vol. 7, pp. 59613–59623, 2019.
[58] A. Garcia-Garcia, S. Orts-Escolano, S. Oprea, V. Villena-Martinez, P. Martinez-Gonzalez, and J. Garcia-Rodriguez, "A survey on deep learning techniques for image and video semantic segmentation," *Appl. Soft Comput.*, vol. 70, pp. 41–65, Sep. 2018.
[59] J. Wu, G. Yang, X. Yang, B. Xu, L. Han, and Y. Zhu, "Automatic counting of *in situ* rice seedlings from UAV images based on a deep fully convolutional neural network," *Remote Sens.*, vol. 11, no. 6, p. 691, Mar. 2019.
[60] Y. Zhao, S. Liu, Z. Hu, Y. Bai, C. Shen, and X. Shi, "Separate degree based Otsu and signed similarity driven level set for segmenting and counting anthrax spores," *Comput. Electron. Agricult.*, vol. 169, Feb. 2020, Art. no. 105230.

DONGYAN ZHANG received the Ph.D. degree from the School of Environment and Resources, Zhejiang University, in 2002. His research interests include remote sensing information processing and analysis, intelligent sensor design and development, and big data mining and application.

ZHICUN WANG is currently pursuing the master's degree with the School of Electronic Information Engineering, Anhui University. His current research interests include computer vision, image processing, and deep learning.

NING JIN received the Ph.D. degree from the Institute of Geographic Sciences and Natural Resources Research, CAS, in 2016. His research interests include remote sensing, crop model, and agricultural information technology.

YU CHEN received the Ph.D. degree from Nanjing Agricultural University, China, in 2009. His major subject is plant disease control fungicide toxicology and resistance. He is also an Expert in disease control of fruit tree industry systems in Anhui, engaged in research on plant disease control, fungicide toxicology, and drug resistance.

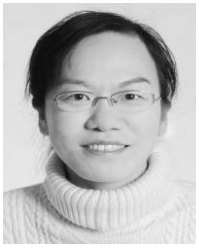

CHUNYAN GU received the M.S. degree from Nanjing Agricultural University, China, in 2008. Her major subject is plant pathology. She currently works as an Assistant Researcher with the Institute of Plant Protection and Agro-Products Safety, Anhui Academy of Agricultural Sciences, Hefei, China, engaged in research on plant disease control.

YANBO HUANG is currently a Research Agricultural Engineer with the U.S. Department of Agriculture-Agricultural Research Service, Crop Production Systems Research Unit. His research interests include aerial application, remote sensing for precision application, soft computing and decision support for precision agriculture, and image processing and process automation.